# Magnetic Properties of $[Ni(dmit)_2]^-$ Anions Induced by Flexible Hydrogen-Bonded Supramolecular Cations $[(p\text{-Xylylenediammonium})_{0.5}(\text{Crown Ethers})]^+$

**Tomoyuki Akutagawa,*,†,‡,§ Asako Hashimoto,‡ Sadafumi Nishihara,‡ Tatsuo Hasegawa,†,‡ and Takayoshi Nakamura*,†,‡,§**

*Research Institute for Electronic Science, Hokkaido University, Sapporo 060-0812, Japan, Graduate School of Environmental Earth Science, Hokkaido University, Sapporo 060-0810, Japan, and PRESTO, Japan Science and Technology Corporation (JST), Kawaguchi 332-0012, Japan*

*Received: July 10, 2002; In Final Form: October 24, 2002*

Flexible supramolecular cation structures, $[(XyDA)_{0.5}(\text{crown ethers})]^+$ complexes, were introduced as countercations to $[Ni(dmit)_2]^-$ anions, which bear an $S = 1/2$ spin, to form novel magnetic crystals (XyDA = *p*-xylylenediammonium, $dmit^{2-}$ = 2-thioxo-1,3-dithiole-4,5-dithiolate, and crown ethers = [12]crown-4, [15]crown-5, or [18]crown-6). Sandwich-type $[(XyDA)_{0.5}(\text{crown ethers})]^+$ structures were formed through hydrogen-bonding interactions in the crystals between the ammonium moieties of XyDA and the oxygen atoms of the crown ethers. [12]Crown-4 yielded three types of $[(XyDA)_{0.5}([12]\text{crown-4})]^+[Ni(dmit)_2]$ polymorphs, whereas two types of $[(XyDA)_{0.5}([15]\text{crown-5})]^+[Ni(dmit)_2]$ polymorphs were obtained using [15]crown-5. Three types of $[(XyDA)_{0.5}(\text{crown ethers})]^+$ structures were identified for these polymorphs. Since the flexible $-CH_2-NH_3^+$ moieties connected to benzene plane have rotational freedom, the $[(XyDA)_{0.5}(\text{crown ethers})]^+$ structures varied according to the conformations of the XyDA cation in the crystals. The larger ring size of [18]crown-6 than that of [12]crown-4 and [15]crown-5 reduced the flexibility of the XyDA cation, and provided only one type of crystal. The $[Ni(dmit)_2]^-$ anion existed as dimer structures, which are in the singlet ground state. The arrangement of the $[Ni(dmit)_2]^-$ anion in the crystals were depended on the structure of $[(XyDA)_{0.5}(\text{crown ethers})]^+$. Correlation of the absolute values of magnetic exchange energy $J$ to the square of the intradimer transfer integral $t^2$ were confirmed.

## 1. Introduction

Polymorphs of crystals, which exhibit different chemical and physical properties due to the changes of intermolecular interactions despite having the same crystal stoichiometry, have been occasionally reported.[1] Polymorphs are related to local potential minima of the crystal lattice energy. Although occurrence of polymorphs cannot be predicted, interesting physical phenomena are often observed in polymorphs. For example, a large number of metals and superconductors have been reported in the partially oxidized bis(ethylenedithiolo)-tetrathiafulvalene (BEDT-TTF) salts, in which the crystals often designated as the polymorph of the α-, $\beta$-, $\theta$-, and $\kappa$-type structures.[2] Molecular superconductors have been typically observed for the $\kappa$-type structures. The $\pi$-electrons of BEDT-TTF molecules can interact both two-dimensionally through the $\pi$-stacks and laterally through S−S contacts of the eight electron-rich S-atoms. The polymorph in BEDT-TTF salts originated from these two-dimensional intermolecular interaction modes. Depending on the intermolecular interaction modes, several types of two-dimensional crystal packing have been observed as a crystal polymorph.

Structural flexibility, in which molecules may change its shape through the rotation of chemical bonds, plays an important role in polymorphism.[3] It has been reported that the ordered and disordered crystal forms in ferrocene were related to the relative orientation of the two cyclopentadienyl rings, which caused a large difference in the crystal system from triclinic, monoclinic, to orthorhombic packing. In the supramolecular assembly level, multiple hydrogen-bonding sites have provided hydrogen-bonded polymorphs.[1,4,5] Diacetimide bearing one proton-donating N−H and two proton-accepting ketone (O═) sites afforded two types of polymorph infinite linear $[-N-H\cdots O=]_\infty$ chain and $[-N-H\cdots O=]_2$ dimer structures),[4] whereas 5,5-diethylbarbituric acid bearing two proton-donating N−H and three proton-accepting O═ sites showed three types of hydrogen-bonded polymorph (infinite single-chain, double-chain, and sheet structures).[5] The synthetic design of intermolecular interaction sites such as hydrogen-bonding sites is important from the point of view of controlling over the complex supramolecular assembly structures.[6]

So far, we have discussed the use of supramolecular cation structures as the countercations to the $[Ni(dmit)_2]$ salts ($dmit^{2-}$ = 2-thioxo-1,3-dithiole-4,5-dithiolate).[7,8] This approach has allowed us to modify the assembled structures of the $[Ni(dmit)_2]^-$ anions, each bearing $S = 1/2$ spin, and thus to adjust the magnetic properties of the $[Ni(dmit)_2]^-$ salts.[8] By using simple $(M^+)(\text{crown ethers})$ and $(M^{2+})(\text{crown ethers})_2$ supramolecules, where $M^+$ and $M^{2+}$ are alkali and alkali earth metals, respectively, a variety of $[Ni(dmit)_2]^-$ anion assemblies, such as monomer, linear one-dimensional Heisenberg chain, dimer chain, and crossed-linear chain, were obtained.[8] Switching from monovalent $M^+$ to divalent $M^{2+}$ cationic systems significantly enhanced the various $[Ni(dmit)_2]^-$ anion assemblies in the

* To whom correspondence should be addressed. Research Institute for Electronic Science, Hokkaido University, N12W6 kita-ku, Sapporo 060-0812, Japan. Phone: +81-11-706-2884. Fax: +81-11-706-4972. E-mail for Dr. T. Akutagawa: takuta@imd.es.hokudai.ac.jp.

† Research Institute for Electronic Science.

‡ Graduate School of Environmental Earth Science.

§ PRESTO.

10.1021/jp026497b CCC: $25.00 
Published on Web 12/10/2002

**SCHEME 1: $[(XyDA)_{0.5}$(crown ethers)$]^+[Ni(dmit)_2]$ Salts**

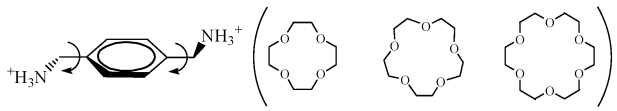

$XyDA^{2+}$(crown ethers)

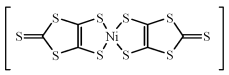

$[Ni(dmit)_2]^-$

**TABLE 1: Crystal Stoichiometry and Shape of Salts 1a−3**

| entry | stoichiometry[a] | shape[a] |
|---|---|---|
| **1a** | $[(XyDA)_{0.5}$([12]crown-4)$]^+[Ni(dmit)_2]$ | plate |
| **1b** | $[(XyDA)_{0.5}$([12]crown-4)$]^+[Ni(dmit)_2]$ | plate |
| **1c** | $[(XyDA)_{0.5}$([12]crown-4)$]^+[Ni(dmit)_2](CH_3CN)$ | plate |
| **2a** | $[(XyDA)_{0.5}$([15]crown-5)$]^+[Ni(dmit)_2]$ | plate |
| **2b** | $[(XyDA)_{0.5}$([15]crown-5)$]^+[Ni(dmit)_2]$ | block |
| **3** | $[(XyDA)_{0.5}$([18]crown-6)$]^+[Ni(dmit)_2]$ | needle |

[a] Determined by X-ray crystal structural analysis.

crystals.[8c] Recently, we have introduced $[Ni(dmit)_2]^-$ salts with a more complicated cation that consist of an organic ammonium cations, such anilinium or *p*-phenylenediammonium, with crown ethers, and have also reported on the formation of a two-legged spin-ladder $[Ni(dmit)_2]^-$ anion chain, induced by the hydrogen-bonded (anilinium)([18]crown-6) supramolecular structure.[9] A slight chemical modification of the cation structures from (anilinium)([18]crown-6) to (*p*-phenylenediammonium)([18]-crown-6)$_2$ was found to modulate the $[Ni(dmit)_2]^-$ anion assemblies, and drastically changed the magnetism from spin-ladder to that of singlet dimer.[10] In the present study, structural flexibility of hydrogen-bonded supramolecular cation structures was further applied to modify the $[Ni(dmit)_2]^-$ anion assemblies in the crystals. Flexible supramolecular cation structures have more conformational freedom than that of simple $M^+$(crown ethers) structures, and cause crystal polymorph and slight modifications of the $[Ni(dmit)_2]^-$ arrangement in the crystals.

To induce the polymorph of $[Ni(dmit)_2]^-$ anion crystals, we introduced the hydrogen-bonding structures between *p*-xylylene-diammonium (XyDA) and [12]crown-4, [15]crown-5, or [18]-crown-6. The XyDA cation has two flexible hydrogen-bonding $-CH_2-NH_3^+$ moieties, which are connected to the benzene ring; these side-chains freely rotate around the C−N bonds (Scheme 1). Since the two $-NH_3^+$ arms form the N−H···O hydrogen-bonds to the oxygen atoms of the crown ethers,[11] the rotational freedom around the C−N bonds can significantly modify the overall cation conformations. Through cation flexibility, the $[Ni(dmit)_2]^-$ anion assemblies and the magnetism of the crystals can also be modified. Herein, we report on the structural and magnetic properties of six new salts: there are two polymorphs of $[(XyDA)_{0.5}$([12]crown-4)$]^+[Ni(dmit)_2]$ (**1a**,**b**), in addition to $[(XyDA)_{0.5}$([12]crown-4)$]^+[Ni(dmit)_2](CH_3CN)$ (**1c**), two polymorphs of $[(XyDA)_{0.5}$([15]crown-5)$]^+[Ni(dmit)_2]$ (**2a**,**b**), and $[(XyDA)_{0.5}$([18]crown-6)$]^+[Ni(dmit)_2]$ (**3**).

## 2. Experimental Section

**2.1. Preparation of $[Ni(dmit)_2]$ Salts.** Table 1 summarizes the crystal stoichiometry and the shape of salts **1a**−**3**. The precursor monovalent $(n\text{-}Bu_4N)[Ni(dmit)_2]$ salt was prepared according to literature.[12] The crystals of salts **1a**−**3** were grown using the standard diffusion method in an H-shaped cell (∼50 mL). The supporting electrolytes $(XyDA)(BF_4)_2$ were synthesized by mixing *p*-xylylenediamine and an aqueous $HBF_4$ solution in MeOH, then recrystallized from $CH_3CN$ (distilled prior to use). The stoichiometry of crystals **1a**−**3** was determined by X-ray structural analysis. The polymorphic crystals were resolved by X-ray structural analysis according to the lattice parameters.

**2.2. Crystal Structure Determination.** Crystallographic data (Table 2) were collected by a Rigaku Raxis-Rapid diffractometer using Mo Kα ($\lambda$ = 0.71073 Å) radiation from a graphite monochromator. Structure refinements were performed using the full-matrix least-squares method on $F^2$. Calculations were performed using Crystal Structure software packages.[13] Parameters were refined using anisotropic temperature factors except for [12]crown-4 and [15]crown-5 in crystals of **1c** and **2b**, respectively, and the hydrogen atom. The positional disorders of [12]crown-4 (**1c**) and [15]crown-5 **B** (**2b**) prevented the application of anisotropic thermal parameters. These molecules were assumed to have disordered arrangements; the hydrogen atoms were excluded from the refinement calculations.

**2.3. Magnetic Susceptibility.** The temperature dependent magnetic susceptibility was measured using a Quantum Design Model MPMS-7 SQUID magnetometer for polycrystalline samples. The applied magnetic field was 1 T for all measure-

**TABLE 2: Crystal Data, Data Collection, and Reduction Parameter of the Salts 1a−3**

| | **1a** | **1b** | **1c** | **2a** | **2b** | **3** |
|---|---|---|---|---|---|---|
| chemical formula | $C_{18}H_{23}NO_4S_{10}Ni$ | $C_{18}H_{23}NO_4S_{10}Ni$ | $C_{20}H_{26}N_2O_4S_{10}Ni$ | $C_{20}H_{27}NO_5S_{10}Ni$ | $C_{20}H_{27}NO_5S_{10}Ni$ | $C_{22}H_{31}NO_6S_{10}Ni$ |
| formula weight | 696.68 | 696.68 | 737.74 | 740.74 | 740.74 | 784.71 |
| space group | $P\bar{1}$ (No. 2) | $P2_1/c$ (No. 14) | $P\bar{1}$ (No. 2) | $P2_1/c$ (No. 14) | $P\bar{1}$ (No. 2) | $P2_1/c$ (No. 14) |
| *a*, Å | 9.1528(7) | 12.163(1) | 8.9020(9) | 9.4437(4) | 11.7931(9) | 10.2585(6) |
| *b*, Å | 12.6654(9) | 16.166(2) | 12.447(1) | 22.398(1) | 16.883(1) | 22.271(1) |
| *c*, Å | 12.8991(7) | 14.550(1) | 15.065(2) | 14.6477(6) | 17.007(2) | 14.3863(8) |
| α, deg | 107.749(2) | | 100.752(4) | | 100.531(4) | |
| *β*, deg | 103.804(3) | 102.825(4) | 103.906(6) | 104.170(2) | 110.223(3) | 94.345(2) |
| *γ*, deg | 91.220(2) | | 104.863(3) | | 100.038(3) | |
| *V*, Å$^3$ | 1375.8(2) | 2789.6(4) | 1510.3(3) | 3004.0(2) | 3018.6(4) | 3277.4(3) |
| Z | 1 | 2 | 2 | 4 | 4 | 4 |
| $D_{calc}$, g cm$^{-1}$ | 1.682 | 1.659 | 1.622 | 1.638 | 1.630 | 1.590 |
| *T* | 297 | 297 | 297 | 100 | 100 | 297 |
| $\mu$, cm$^{-1}$ | 14.91 | 14.71 | 13.64 | 13.74 | 13.67 | 12.66 |
| reflctns measured | 6248 | 6549 | 6319 | 7042 | 12603 | 7704 |
| independent reflctns | 6248 | 6330 | 6319 | 6858 | 12603 | 7501 |
| reflctns used | 4906 | 2267 | 2874 | 4714 | 9832 | 4636 |
| $R^{a)}$ | 0.051 | 0.040 | 0.086 | 0.048 | 0.099 | 0.041 |
| $R_w(F^2)^{a)}$ | 0.062 | 0.067 | 0.048 | 0.089 | 0.102 | 0.063 |
| GOF | 1.19 | 1.19 | 0.07 | 1.07 | 0.04 | 1.13 |

[a] $R = \Sigma||F_o| - |F_c||/\Sigma|F_o|$ and $R_w = (\Sigma\omega(|F_o| - |F_c|)^2/\Sigma\omega F_o^2)^{1/2}$.

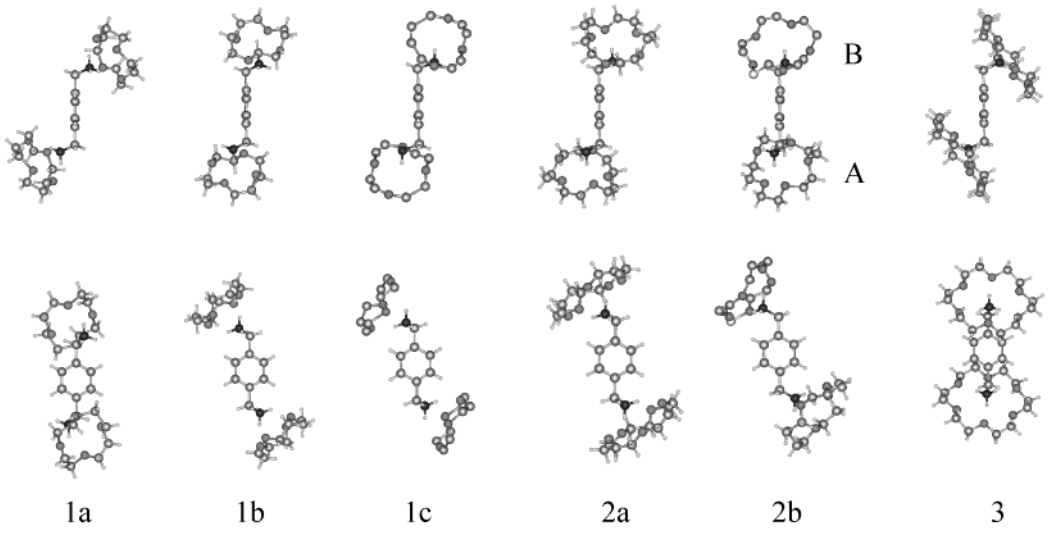


**Figure 1.** $[(XyDA)_{0.5}(\text{crown ethers})]^+$ structures of salts **1a**−**3** viewed parallel (top) and normal (bottom) to the benzene plane. Two types of crystallographically independent [15]crown-5 (**A** and **B**) were observed for salt **2b**.

ments. Magnetic susceptibilities of the polymorphs were independently measured for each separated crystal. The magnetic measurements of salt **1c** could not be carried out due to the scarcity of crystals (less than 0.1 mg).

**2.4. Calculation of Transfer Integrals.** The transfer integrals $t$ were calculated within the tight-binding approximation using the extended Hückel molecular orbital method. The LUMO of the $[Ni(dmit)_2]$ molecule was used as the basis function.[14] Semiempirical parameters for Slater-type atomic orbitals were obtained from literature.[14] The $t$ values between each pair of molecules were assumed to be proportional to the overlap integral $S$ via the equation $t = -10S$ eV.

## 3. Results and Discussion

Salts **1a** and **1b** have the same stoichiometry of $[(XyDA)_{0.5}([12]\text{crown-4})]^+[Ni(dmit)_2]$, whereas salt **1c**, with an $CH_3CN$ molecule, had a stoichiometry of $[(XyDA)_{0.5}([12]\text{crown-4})]^+[Ni(dmit)_2](CH_3CN)$. The crystal symmetry of salt **1b** ($P2_1/c$) was higher than those of salts **1a** ($P\bar{1}$) and **1c** ($P\bar{1}$), whose $[Ni(dmit)_2]^-$ arrangements were completely different from each other. Salts **2a** and **2b** had crystal symmetry of $P2_1/c$ and $P\bar{1}$, respectively, with identical stoichiometry of $[(XyDA)_{0.5}([15]\text{crown-5})]^+[Ni(dmit)_2]$. The $[Ni(dmit)_2]^-$ anion assemblies and magnetism of these two salts were also rather different from each other. Only one type of crystal containing [18]crown-6 was obtained as $[(XyDA)_{0.5}([18]\text{crown-6})]^+[Ni(dmit)_2]$ (**3**).

The LUMO of $[Ni(dmit)_2]^-$ anion was occupied by one electron bearing S = 1/2 spin. The magnetism of crystals was determined by the magnetic exchange energy ($J$), which was proportional to the square of transfer integral $t^2$, i.e., magnitude of intermolecular interaction. In general, the $[Ni(dmit)_2]^-$ anions have $\pi-\pi$ interactions, in which the magnitude varied according to the cation structures. The appearances of polymorphs in salts **1** and **2** were explained using the conformational differences in the supramolecular cation structures, and thus we first discuss the differences in the cation structure from the structural point of view.

**3.1. Cation Conformations.** Figure 1 summarizes the supramolecular cation structures of salts **1a**−**3**, which were composed of sandwich-type $[(XyDA)_{0.5}(\text{crown ethers})]^+$. An inversion center existed for the XyDA molecules, except for salt **2b**. Salt **2b** had two types of crystallographically independent [15]crown-5 molecules (**A** and **B**). The two $-CH_2-NH_3^+$ arms of the XyDA unit formed N−H···O hydrogen bonds to the oxygen atoms of crown ethers, resulting in similar types of supramolecular structures. When the structures were viewed parallel (Figure 1, top) and normal (Figure 1, bottom) to the benzene plane, the hydrogen-bonding conformation of the XyDA cation for crown ethers slightly changed from cation to cation. These differences in cation conformation were directly related to the $[Ni(dmit)_2]^-$ arrangement.

**SCHEME 2: Structural Parameters of $[(XyDA)_{0.5}(\text{crown ethers})]^+$ Unit**

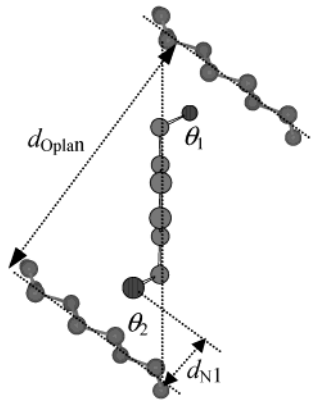


The conformational differences of the $[(XyDA)_{0.5}(\text{crown ethers})]^+$ structures are represented by selected structural parameters ($d_{N1}$, $\theta_1$, $\theta_2$, and $d_{Oplane}$, which are the deviation distance of nitrogen atom from the mean O-plane of crown ether, the dihedral angle of the C═C−C−N bonds of XyDA, the dihedral angle between mean O-plane and benzene $C_6$-plane, and the distance between the mean O-plane of the two crown ethers, respectively, as shown in Scheme 2). These structural parameters and selective hydrogen-bonded N−O distances are tabulated in Table 3.

Effective N−H···O hydrogen bonding between the two $-NH_3^+$ groups and the oxygen atoms of [12]crown-4 were observed for salts **1a**−**c**. The observed N−O hydrogen-bonding distances ranged from 2.780(4) to 2.96(1) Å, in which the average N−O distance for salts **1a**, **1b**, and **1c** were 2.85, 2.88, and 2.89 Å, respectively. Since the magnitude of the N−O distances were comparable to the standard N−O hydrogen-bonding distance (2.87 Å),[15] the $[(XyDA)_{0.5}([12]\text{crown-4})]^+$

**TABLE 3: Structural Parameters of Cation Units for Salts 1a−3[a]**

| | 1a | 1b | 1c | 2a | 2b A, B | 3 |
|---|---|---|---|---|---|---|
| N1−O1 | 2.780(4) | 2.876(7) | 2.96(1) | 2.841(4) | 2.822(8), 2.77(1) | 2.874(4) |
| N1−O2 | 2.853(4) | 2.870(7) | 2.893(9) | 2.987(5) | 2.822(7), 2.71(1) | 2.880(4) |
| N1−O3 | 2.923(4) | 2.883(8) | 2.869(9) | 2.939(5) | 3.010(7), 3.14(1) | 2.853(4) |
| N1−O4 | 2.855(4) | 2.898(7) | 2.84(1) | 2.871(4) | 2.955(7), 3.23(1) | 2.915(4) |
| N1−O5 | | | | 2.854(5) | 2.976(7), 2.79(1) | 2.870(4) |
| N1−O6 | | | | | | 2.843(4) |
| $N1-O_{AV}$ | 2.85 | 2.88 | 2.89 | 2.90 | 2.92 | 2.87 |
| $d_{N1}$ | 2.08 | 2.08 | 2.09 | 1.70 | 1.60 | 0.68 |
| $\theta_1$ | 64.3(6) | 52.4(8) | 61.2(1) | 51.0(6) | 28.8(1), 21.9(1) | 83.6(5) |
| $\theta_2$ | 37.4 | 87.2 | 81.2 | 85.9 | 67.5, 74.3 | 36.3 |
| $d_{Oplane}$ | 8.40 | 10.41 | 9.48 | 9.89 | 10.46 | 8.22 |

[a] The parameters $d_{N1}$, $\theta_1$, $\theta_2$, and $d_{Oplane}$ were defined in Scheme 2.

structures were constructed using the moderate strength of eight $NH_3^+-O$ hydrogen-bonding interactions. Small cavity-size of [12]crown-4 deviated the nitrogen atom upward toward the mean O4-plane of [12]crown-4, in which the $d_{N1}$ distances for salts **1a**, **1b**, and **1c** were 2.08, 2.08 and 2.09 Å, which were comparable to those for $(NH_4^+)([12]crown-4)[Ni(dmit)_2]_3$ ($d_{N1}$ = 2.05 Å).[7g] Dihedral angles $\theta_1$ of the XyDA unit of salts **1a**, **1b**, and **1c** were calculated as 64.3(6), 61.2(1), and 52.4(8)°, respectively, whereas a large difference was detected for dihedral angle $\theta_2$ between the [12]crown-4 $O_4$-plane and benzene $C_6$-plane. Values for angle $\theta_2$ for salts **1a**, **1b**, and **1c** were 37.4, 87.2, and 81.2°, respectively. The $d_{Oplane}$ distance of salt **1** increased ∼1 Å, in the order **1a** ($d_{Oplane}$ = 8.40 Å), **1c** ($d_{Oplane}$ = 9.48 Å), and **1b** ($d_{Oplane}$ = 10.40 Å), which significantly modified the cation−$[Ni(dmit)_2]^-$ anion arrangements.

As shown in Figure 1, close resemblances can be seen between the cation conformations of salts **2a**,**b**. For salt **2a**, effective N−O hydrogen-bonding were observed within distances between 2.841(4) to 3.010(7) Å. For salt **2b**, two types of independent N−O interactions for [15]crown-5 **A** and **B** were observed; N−O hydrogen-bonding distances between the XyDA and [15]crown-5 **A** were detected at distances between 2.822-(8) to 3.010(7) Å. The disorder of [15]crown-5 **B** provided three strong N−O interactions (2.71(1), 2.77(1), and 2.79(1) Å) and two weak interactions (3.14(1) and 3.23(1) Å). The average N−O distance of 2.92 Å in salt **2b** was slightly longer than that of salt **1**; thus, the hydrogen-bonded supramolecules of salts **2a**,**b** have subtle loose structures. Significantly larger cavity diameter of [15]crown-5 than that of [12]crown-4 decreased the $d_{N1}$ distances, whose values for salts **2a**,**b** were 1.7 and 1.6 Å, respectively. The values for dihedral angle $\theta_1$ of salt **2b** (28.8-(1) and 21.9(1)°) were half of the value for salt **2a** ($\theta_1$ = 51.0-(6)°), and greatly changed the conformations of the XyDA structures. However, these structural differences of XyDA were minimized due to the difference of values for angle $\theta_2$ of salts **2a** (85.9°) and **2b** (67.5 and 74.3°), which resulted in the small difference of $d_{Opalne}$ for salts **2a** (9.89 Å) and **2b** (10.46 Å).

One stable conformation was detected for the $[(XyDA)_{0.5}$-([18]crown-6)$]^+$ structure. Twelve N−H···O hydrogen bonds within distances from 2.843(4) to 2.915(4) Å held the cation structure. The average N−O hydrogen-bonding distance of 2.87 Å was consistent with the standard N−O hydrogen-bonding distance.[15] The supramolecular cation was constructed from the moderate strengths of hydrogen-bonding interactions. Due to the larger cavity diameter of [18]crown-6 than those of [12]-crown-4 and [15]crown-5, the $-NH_3^+$ moiety penetrated deeper into the cavity, whose $d_{N1}$ distance was 0.68 Å. The dihedral angle $\theta_1$ of 83.6(5)° was nearly a right angle, whereas angle $\theta_2$ of 36.3° was comparable to that of salt **1a**. [18]crown-6 planes were much inclined to the $\pi$-plane of XyDA, which covered the $\pi$-plane of XyDA. The $d_{Oplane}$ of 8.22 Å of salt **3** resembled that of salt **1a**. The small $\theta_2$ angle for salts **1a** and **3** provided a similar type of cation−$[Ni(dmit)_2]^-$ arrangement. A subtle conformational change in the $[(XyDA)_{0.5}(crown\ ethers)]^+$ units resulted in the polymorphs.

**3.2. Cation−$[Ni(dmit)_2]^-$ Anion Arrangement.** The crystal lattice energy of salts **1a**−**3** was basically determined using Madelung energy due to the ionic molecules of XyDA and $[Ni(dmit)_2]^-$ anion.[16] Conformational changes of the cation structures led to the modification of the molecular packing between the XyDA cation and $[Ni(dmit)_2]^-$ anion, which yielded the crystal polymorphs.

The relative positions of the XyDA cation and $[Ni(dmit)_2]^-$ anion, viewed normal to the $[Ni(dmit)_2]^-$ plane and short axis of $[Ni(dmit)_2]^-$, are summarized in Figure 2. Two S−C distances [S(1)−C(16) = 3.698(3) and S(1)−C(15) = 3.772(3) Å] were observed for salt **1a**, whereas three S−C contacts [S(1)−C(22) = 3.750(4), S(2)−C(22) = 3.622(4), and S(1)−C(21) = 3.670(4) Å] were observed for salt **3**. Since the dihedral angle between the $\pi$-planes of XyDA and $[Ni(dmit)_2]^-$ of salt **1a** (24.7 degree) was different than that of salt **3** (81.5°), the arrangements of $[Ni(dmit)_2]^-$ anion in salts **1a** and **3** were significantly different from each other. The $\pi-\pi$ stacking intermolecular interactions between the XyDA cation and $[Ni(dmit)_2]^-$ anion were not observed for salts **1a** and **3**. The shorter $d_{Oplane}$ distances of salts **1a** (8.40 Å) and **3** (8.22 Å) than those of other salts were insufficient to allow the formation of $\pi-\pi$ overlap through the introduction of the $[Ni(dmit)_2]^-$ anion into the space sandwiched between two crown ethers.

Among the four intermolecular distances of salt **1b** that were less than 3.8 Å [S(2)−C(15) = 3.779(6), S(2)−C(15)′ = 3.646-(6), S(2)−C(16) = 3.559(6), and S(2)−C(17) = 3.491(5) Å], the S(2)−C(17) contact was shorter than the van der Waals contact.[17] Although the spiral $[Ni(dmit)_2]^-$ arrangements along the $2_1$-axis disturbed the formation of the $\pi-\pi$ overlap in salt **1b**, the larger $d_{Oplane}$ value of salt **1b** ($d_{Oplane}$ = 10.40 Å) than those of **1a** ($d_{Oplane}$ = 8.40 Å) and **1c** ($d_{Oplane}$ = 9.48 Å) allowed the insertion of the lateral sulfur atom into the space sandwiched between two [12]crown-4 ether planes.

For salts **1c**, **2a**,**b**, $\pi-\pi$ interactions between the $\pi$-planes of the $[Ni(dmit)_2]^-$ anion and the benzene moiety were observed as cation−$[Ni(dmit)_2]^-$ arrangements. The $\pi$-planes of XyDA overlapped with the $\pi$-planes of $[Ni(dmit)_2]^-$ anion, and were nearly parallel to each other. The existence of bulky crown ethers yielded the $\pi$-stacking structure at the outer five-membered ring of the $[Ni(dmit)_2]^-$ anion.

Rotational freedom around the C−N bonds of XyDA dication and hydrogen bonding between ammonium moieties of XyDA and the crown ether generated a variety of $[(XyDA)_{0.5}(crown\ ethers)]^+$ conformations.

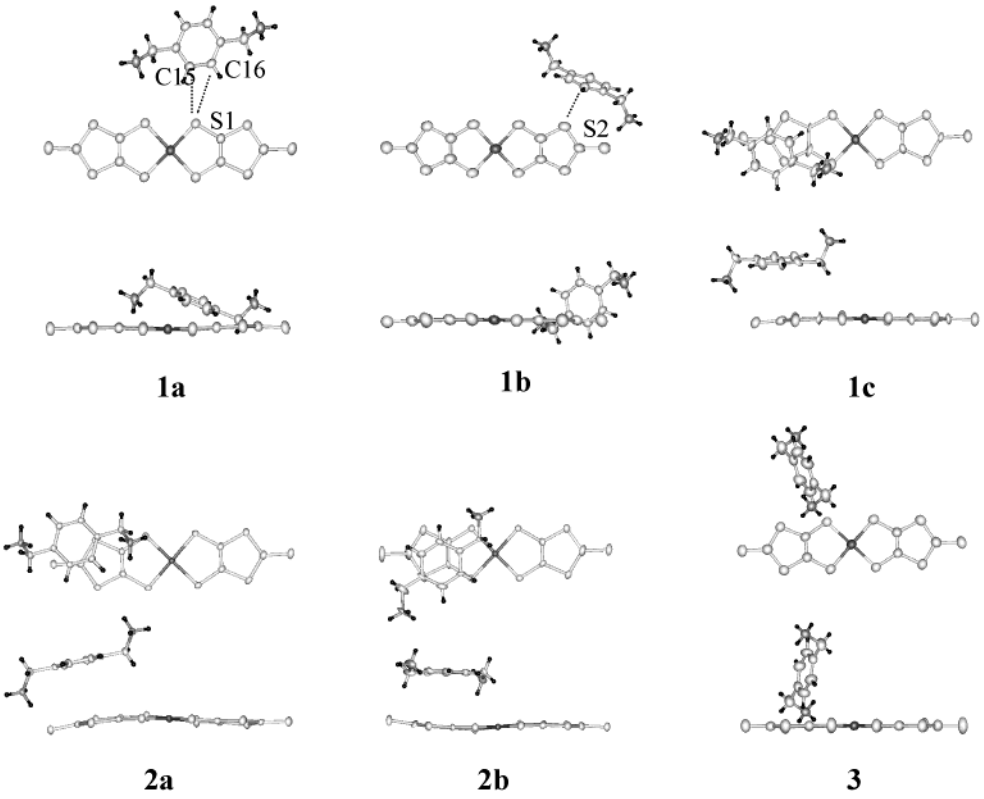


**Figure 2.** XyDA cation−$[Ni(dmit)_2]^-$ anion arrangements. The S−C distances shorter than 3.8 Å in salt **1a**: S(1)−C(16) = 3.698(3) and S(1)−C(15) = 3.772(3) Å. Salt **1b**: S(2)−C(15) = 3.779(6), S(2)−C(15)′ = 3.646(6), S(2)−C(16) = 3.559(6), S(2)−C(17) = 3.491(5) Å. Salt **1c**: S(6)−C(7) = 3.74(2), S(1)−C(9) = 3.62(2), S(7)−C(9) = 3.71(2) Å. Salt **2a**: S(3)−C(7) = 3.791(5), S(4)−C(8) = 3.778(4), S(4)−C(10) = 3.743(4) Å. Salt **2b**: S(12)−C(15) = 3.771(5), S(14)−C(17) = 3.793(5), S(17)−C(15) = 3.754(5), S(18)−C(14) = 3.621(5), S(19)−C(16) = 3.678(4), S(12)−C(14) = 3.567(5), S(14)−C(18) = 3.734(5), S(19)−C(19) = 3.627(4) Å. Salt **3**: S(1)−C(22) = 3.750(4), S(2)−C(22) = 3.622(4), S(1)−C(21) = 3.670(4) Å.

**TABLE 4: Transfer Integral ($t \times 10^{-2}$ eV)[a] and Magnetic Parameters in Salts 1a−3**

| | 1a | 1b | 1c | 2a | 2b | 3 |
|---|---|---|---|---|---|---|
| $t_1$ | 10.7 | 5.50 | 5.47 | 7.45 | 4.58 | 8.29 |
| $t_2$ | 2.45 | 0.47 | 0.45 | 1.50 | 0.71 | 0.86 |
| $t_3$ | | | | | 0.95 | |
| $J/k_B$, K | −315 | −64 | | −132 | | −84 |
| magnetism[b] | S−T | S−T | | S−T | C−W | S−T |
| $C$, emu K mol$^{-1}$ | 0.352 | 0.381 | | 0.374 | 0.355 | 0.384 |
| $\theta$, K | | | | | −8.6 | |

[a] The transfer integrals ($t$) were obtained by the LUMO of $[Ni(dmit)_2]^-$ based on the extended Hückel calculation ($t = -10S$ eV; $S$ is overlap integral). [b] S−T and C−W are singlet−triplet thermal excitation and Curie−Weiss model, respectively.

**3.3. $[Ni(dmit)_2]^-$ Anion Arrangements and Magnetism.** Each $[Ni(dmit)_2]^-$ anion has one $S = 1/2$ spin, and the assemblies are directly related to the magnetism. Transfer integrals based on the extended Hückel molecular orbital calculations were employed to evaluate the magnitude of intermolecular interaction of $[Ni(dmit)_2]^-$ anions. The magnetic exchange energy $J$ is proportional to the square of transfer integral,

$$J = \frac{2t^2}{U_{\text{eff}}} \quad (1)$$

in which $U_{\text{eff}}$ is the effective on-site Coulomb repulsive energy in the solid.[18] The magnetism of salts **1a**−**3**, based on the $t$ values between nearest neighboring $[Ni(dmit)_2]^-$ molecules, will be discussed. Table 4 summarizes transfer integral ($t \times 10^{-2}$ eV) and magnetic parameters in salts **1a**−**3**.

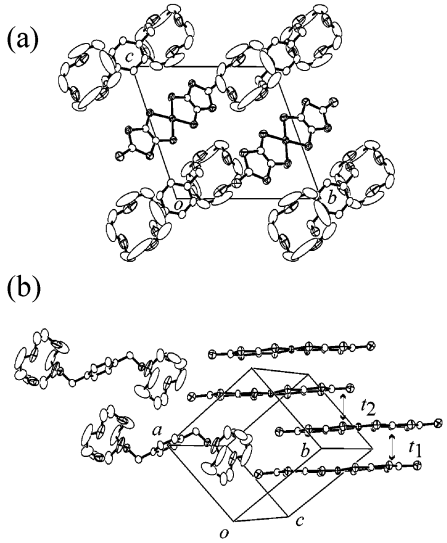


**Figure 3.** Crystal structures of salt **1a**. Unit cell viewed along the *a*-axis (a). $[Ni(dmit)_2]^-$ dimer stack and $[(XyDA)_{0.5}([12]crown-4)]^+$ stack viewed along the short axis of $[Ni(dmit)_2]^-$ (b). Intermolecular transfer integrals (intradimer $t_1$ and interdimer $t_2$) are shown.

*3.3.1. Salts **1a**−**c**.* The change in $[(XyDA)_{0.5}([12]crown-4)]^+$ conformation of salts **1** influenced the $[Ni(dmit)_2]^-$ assemblies in the crystals. Figure 3a shows the unit cell of salt **1a**, viewed along the *a*-axis. Segregated stacking structure of $[Ni(dmit)_2]^-$ anions was observed along the *a*-axis. Similarly segregated stacking structures are often observed in highly electrical conducting salts through formation of a $\pi$-band structure. In general, monovalent $[Ni(dmit)_2]^-$ anion has a tendency to form

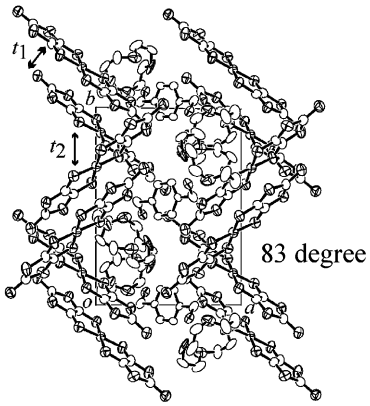


**Figure 4.** Crystal structure of salt **1b**. Unit cell viewed along the *c*-axis. Intermolecular interaction modes (intradimer $t_1$ and interdimer $t_2$) are shown.

a mixed-stack structure between the cation and $[Ni(dmit)_2]^-$ anion. Electrostatic repulsive energy between the $[Ni(dmit)_2]^-$ anions was disadvantageous in forming segregated stacks. From this point of view, the crystal structure of salt **1a** was rather unusual. In the $[Ni(dmit)_2]^-$ stack (Figure 3b), the $\pi-\pi$ dimer was observed as the basic structural unit. Comparatively, the intradimer transfer integral $t_1$ ($10.7 \times 10^{-2}$ eV) was five times larger than the interdimer $t_2$-interaction ($2.45 \times 10^{-2}$ eV). The magnetic interaction was basically dominated by the intradimer $t_1$-interaction. Each $[Ni(dmit)_2]^-$ stack was isolated within the crystal by the surrounding stacks of $[(XyDA)_{0.5}([12]crown\text{-}4)]^+$ cations along *the a*-axis.

Although possessing the same crystal stoichiometry, the $[Ni(dmit)_2]^-$ anion arrangement for salt **1b** was completely different to that of salt **1a**. Figure 4 shows the unit cell of salt **1b** viewed along the *c*-axis. The basic unit for salt **1b** was the $\pi-\pi$ dimer of $[Ni(dmit)_2]^-$ anion, which was similar to that for salt **1a**. However, due to the difference of cation−anion arrangement, the segregated stacking structure of dimers was not observed. The intradimer $t_1$-interaction ($5.54 \times 10^{-2}$ eV) was half of that for the $\pi-\pi$ dimer of salt **1a**. The $[Ni(dmit)_2]^-$ anions inclined at an angle of 83 degree along the spiral $2_1$-axis. Each $[Ni(dmit)_2]^-$ dimer interacted through weak lateral S−S contacts ($t_2 = 0.47 \times 10^{-2}$ eV) along the *b*-axis. Between the $[Ni(dmit)_2]^-$ chains, the $[(XyDA)_{0.5}([12]crown\text{-}4)]^+$ cations were introduced via S−$\pi$ intermolecular interactions.

Since salt **1c** was shown to contain one $CH_3CN$ molecule in the crystal, strictly speaking this salt is not a polymorph of salts **1a**,**b**. Figure 5a shows the unit cell viewed along the *a*-axis. The basic structural unit was the $[Ni(dmit)_2]^-$ anion $\pi-\pi$ dimer, which is a common structural property for salt **1**. The intradimer $t_1$-interaction ($5.47 \times 10^{-2}$ eV) was similar in magnitude to that of salt **1b**. Weak lateral S−S contacts were observed along the *a*-axis (Figure 5b), whose $t_2$-interaction of $0.45 \times 10^{-2}$ eV was ineffective in increasing the magnetic interaction between the dimers. Since each $[Ni(dmit)_2]^-$ has a $\pi-\pi$ interaction with the XyDA cation, the interdimer interaction was perturbed along the *c*-axis.

The crystal structures of salts **1a**,**b** showed that the intermolecular interaction within the $[Ni(dmit)_2]^-$ anion dimer was the most dominant in the crystals. Figure 6 illustrates the temperature-dependent molar magnetic susceptibilities $\chi_{mol}$ per one $[Ni(dmit)_2]^-$ anion for salts **1a**,**b**. By increasing the temperature from 4 to 350 K, a broad maximum of the magnetic susceptibilities for salts **1a** and **1b** were obtained at around 80 and 350 K, respectively. $S = 1/2$ spins on $[Ni(dmit)_2]^-$ anion directly interacted to each other in the dimer. In general, these

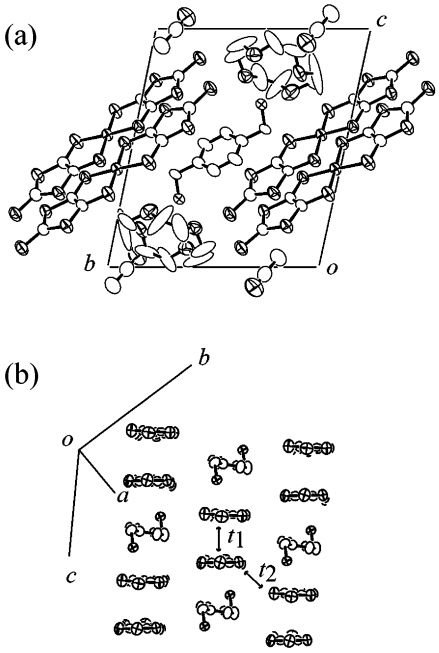


**Figure 5.** Crystal structures of salt **1c**. Unit cell viewed along the *a*-axis (a). Intermolecular interaction modes (intradimer $t_1$ and interdimer $t_2$) viewed along the long axis of $[Ni(dmit)_2]^-$ are shown (b). For clarity, [12]crown-4 molecules are omitted from the figures.

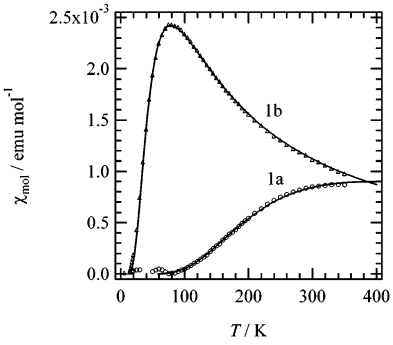


**Figure 6.** Temperature-dependent molar magnetic susceptibility ($\chi_{mol}$ per one $[Ni(dmit)_2]^-$ anion) of salts **1a**,**b**. The solid lines represent the fit using eq 2 (see text).

$[Ni(dmit)_2]^-$ dimer provided a spin singlet ground state, and therefore we applied the single−triplet thermal excitation model for magnetism for salts **1a**,**b**,[19]

$$\chi_{mol} = \frac{C}{T}\frac{(4\exp(2J/k_BT))}{(1+3\exp(2J/k_BT))} \qquad (2)$$

where $C$, $J$, and $k_B$ are Curie constant, magnetic exchange energy, and Boltzmann constant, respectively. The temperature-dependent magnetism of salts **1a**,**b** was fitted using eq 2, in which the $J$ values of salts **1a** and **1b** were −315 and −64 K, respectively. The absolute magnitude of $J$ values corresponded to the thermal excitation energy from singlet to triplet spin state on the $[Ni(dmit)_2]^-$ anion dimer. The $J$ value of salt **1a** was roughly 5 times larger than that of salt **1b**, where the difference of the $J$ values was explained using the difference in the dimerization magnitude $t_1$. Conformational changes in the flexible hydrogen-bonded supramolecular cations largely modified the $[Ni(dmit)_2]^-$ arrangement and magnetic exchange energy. Values for $C$ for salts **1a** and **1b** were 0.352 and 0.381 emu K mol$^{-1}$, respectively, in which the magnitude was consistent with one $S = 1/2$ spin per $[Ni(dmit)_2]^-$ anion.

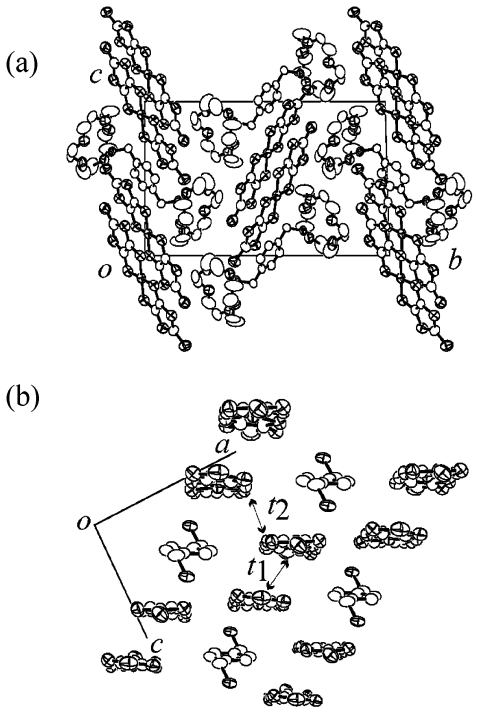


**Figure 7.** Crystal structures of salt **2a**. Unit cell viewed along the *a*-axis (a). Intermolecular interaction modes (intradimer $t_1$ and interdimer $t_2$) viewed along the long axis of $[Ni(dmit)_2]^-$ are shown (b). For clarity, [15]crown-5 molecules are omitted from the figures.

The crystal structures of salts **1a** and **1b** implied relatively large interdimer magnetic exchange energy. However, from eq 1, the magnetic anisotropy between intra- and interdimer, $J_1/J_2$, of salts **1a** and **1b** was estimated as 120 and 20, respectively. Such large anisotropy values indicated that the $t_2$-interactions in the crystals of **1a** and **1b** were negligible, and thus we can safely apply eq 2 to explain the magnetism of **1a**,**b**.

*3.3.2. Salts **2a** and **2b**.* The $[Ni(dmit)_2]^-$ arrangements for salts **2a**,**b** differed significantly between each other; furthermore, two crystallographically independent $[Ni(dmit)_2]^-$ anions (**A** and **B**) were observed for salt **2b**. For both salts, $\pi-\pi$ overlap was observed as the cation$-[Ni(dmit)_2]^-$ anion arrangement. The crystal structure of salt **2a** resembled that of salt **1c**. Figure 7a shows the unit cell viewed along the *a*-axis. The basic structural unit was the $\pi-\pi$ dimer of the $[Ni(dmit)_2]^-$ anions, whose $t_1$-interaction ($7.45 \times 10^{-2}$ eV) was roughly 40% larger than that of salt **1c** ($5.47 \times 10^{-2}$ eV). The spiral $2_1$-axis isolated each dimer along the *b*-axis; weak $t_2$-interactions ($1.50 \times 10^{-2}$ eV) through the lateral S$-$S contacts were observed along the *c*-axis. The $\pi$-plane of XyDA was sandwiched between the $[Ni(dmit)_2]^-$ anion dimers along the $+a-c$-axis (Figure 7b), in which the packing resembled that of salt **1c**. Both $t_1$- and $t_2$-interactions for salt **2a** were larger than those of salt **1c**, thus increasing the ring-size from [12]crown-4 to [15]crown-5 enhanced the intermolecular interaction between the $[Ni(dmit)_2]^-$ anions.

Due to the existence of two types of $[Ni(dmit)_2]^-$ anions (**A** and **B**), the crystal structure of salt **2b** was significantly more complicated than that of salt **2a**. Figure 8 shows the unit cell viewed along the long axis of $[Ni(dmit)_2]^-$ **A**. The cation$-[Ni(dmit)_2]^-$ **A** anion arrangement was $\pi-\pi$ interaction, which was similar to that of salts **1c** and **2a**. In contrast, the $[Ni(dmit)_2]^-$ **B** anion was isolated from the XyDA anion, and instead of the $\pi-\pi$ dimer arrangement of the $[Ni(dmit)_2]^-$ anions, lateral **B**$-$**B** dimer was observed at the intradimer $t_1$-interaction of $4.58 \times 10^{-2}$ eV. Weak interdimer $t_2$-interaction ($0.71 \times 10^{-2}$ eV) connected each dimer along the *c*-axis, whereas weak $t_3$-interaction ($0.95 \times 10^{-2}$ eV) between the **A** and **B** anions was observed along the *b*-axis. Since both $t_2$- and $t_3$-interactions were ineffective in increasing the magnetic interactions in the crystal, the magnetism of salt **2b** was dominated by the lateral **B**$-$**B** dimer.

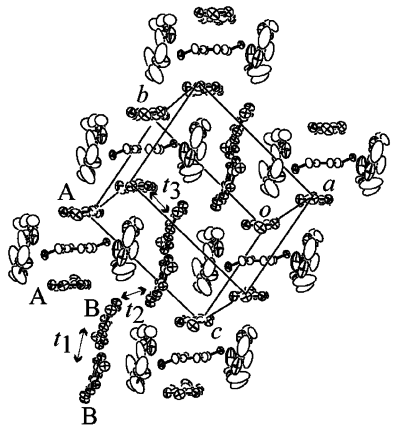


**Figure 8.** Crystal structure of salt **2b**. Unit cell viewed along the long axis of $[Ni(dmit)_2]^-$ **A**. Two types of $[Ni(dmit)_2]^-$ (**A** and **B**) were observed. Intermolecular interaction modes ($t_1-t_3$) are shown.

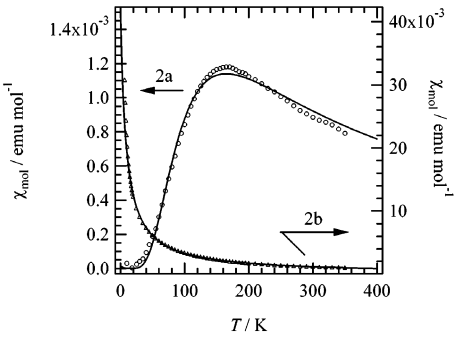


**Figure 9.** Temperature-dependent molar magnetic susceptibility ($\chi_{mol}$) per one $[Ni(dmit)_2]^-$ anion for salts **2a**,**b**. The solid lines represent the results predicted using eq 2 and Curie$-$Weiss behavior (see text).

The temperature-dependent magnetic susceptibility of salts **2**,**b** were significantly different from each other (Figure 9), which can be related to the difference between the $[Ni(dmit)_2]^-$ anion dimer arrangements. The crystal structural analysis of salts revealed the formation of $[Ni(dmit)_2]^-$ anion $\pi-\pi$ dimer for salt **2a**, whereas salt **2b** was composed of laterally interacted **B**$-$**B** dimer and isolated **A**. The magnetic susceptibility of salt **2a** exhibited a broad maximum at around 150 K, whereas that of salt **2b** conformed to the Curie$-$Weiss equation. The magnetism of salt **2a** fitted well to eq 2, whose magnetic parameters $C$ and $J$ were 0.374 emu K mol$^{-1}$ and $-132$ K, respectively. A large value for magnetic anisotropy $J_1/J_2 = 25$, estimated from the $t_1$- and $t_2$-interactions, implied an isolated dimer structure for salt **2a**. The temperature-dependent magnetism of salt **2b** can be explained using the Curie$-$Weiss behavior, in which the magnetic parameters $C$ and Weiss temperature were 0.355 emu K mol$^{-1}$ and $-8.6$ K, respectively. The lateral S$-$S interaction ($t_1 = 4.58 \times 10^{-2}$ eV) of salt **2b** was weaker than the intradimer $\pi-\pi$ interactions of salts **1a**,**b**, and **2a**, which reflected the magnetism of the nearly free $S = 1/2$ spin state of salt **2b**. From the magnitude of transfer integrals $t_1-t_3$, the antiferromagnetic interaction was dominated by the lateral **B**$-$**B** dimer. The $S = 1/2$ spin in $(NH_4^+)$([15]crown-5)-$[Ni(dmit)_2]$ and $(Ca^{2+})$([15]crown-5)$_2[Ni(dmit)_2]_2$ salts behaved as free spin following the Curie$-$Weiss equation, whose crystal

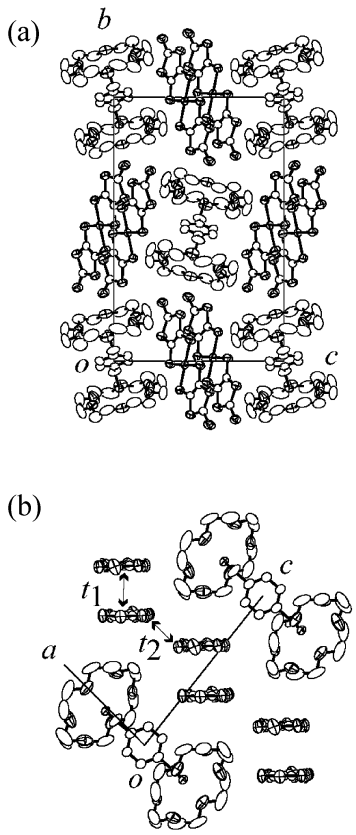


**Figure 10.** Crystal structures of salt **3**. Unit cell viewed along the *a*-axis (a). Intermolecular interaction modes (intradimer $t_1$ and interdimer $t_2$) viewed along the long axis of $[Ni(dmit)_2]^-$ anion are shown (b).

structures were composed of $\pi-\pi$ $Ni(dmit)_2]^-$ anion dimer.[8c,d] The $[Ni(dmit)_2]^-$ anion dimerization magnitude of $(NH_4^+)$([15]-crown-5)$[Ni(dmit)_2]$ and $(Ca^{2+})$([15]crown-5)$_2[Ni(dmit)_2]_2$ salts were also less than $\sim 5 \times 10^{-2}$ eV. The $t_1$-interaction ($4.58 \times 10^{-2}$ eV) of salt **2b** was too weak in forming the singlet state within the measurable temperature range.

*3.3.3. Salt 3.* The larger [18]crown-6 molecule prevented the formation of $\pi-\pi$ overlap between the cation and $[Ni(dmit)_2]^-$ anion. Figure 10a shows the unit cell viewed along the *a*-axis. The basic structural unit of the $[Ni(dmit)_2]^-$ anion was the $\pi-\pi$ dimer, in which the intradimer $t_1$-interaction ($8.29 \times 10^{-2}$ eV) was larger than those of salts **1b**,**c**, and **2a**, and smaller than that of salt **1a**. The $[Ni(dmit)_2]^-$ anion dimers and XyDA cations were located alternately along the *b*- and *c*-axes. Along the *b*-axis, the alternate arrangement of $[(XyDA)_{0.5}([18]crown-6)]^+$ and $[Ni(dmit)_2]^-$ prevented the direct $[Ni(dmit)_2]^-$ interdimer interaction. Weak lateral $t_2$-interaction ($0.86 \times 10^{-2}$ eV) was observed along the *a*-axis (Figure 10b), and was ineffective in increasing the magnetic interaction.

The temperature-dependent magnetic susceptibility of salt **3** was similar to those of salts **1a**,**b**, and **2a**. A broad maximum of magnetic susceptibility was observed at around 100 K, in which the temperature-dependent behavior was well fitted using eq 2. The magnetic parameters of *C* and *J* were 0.384 emu K $mol^{-1}$ and $-84$ K, respectively. Relatively weak interdimer $t_2$-interaction resulted in magnetic anisotropy $J_1/J_2 = 100$. The formation of a strong $[Ni(dmit)_2]^-$ anion dimer was consistent with the magnetism of the dimer model.

**3.4. Magnetic Exchange Energy and Transfer Integral.** In the case where the conduction band was partially filled, the $[Ni(dmit)_2]$ crystal was observed to function as a conductor, whose bandwidth $4t$ ($\sim$1 eV) was comparable to typical $U_{eff}$ in a molecular solid. In fully charge transferred states, electrons tend to localize on the $[Ni(dmit)_2]^-$ anion sites. As observed for salts **1a**$-$**3**, in most cases, $[Ni(dmit)_2]^-$ anions formed dimers, and the salts acted as insulators. The magnetic exchange energy *J* between the localized spins was defined by eq 1. Since the intradimer transfer integral $t_1$ in the crystal was one of the useful parameters in evaluating intermolecular magnetic exchange energy, we constructed a variety of $[Ni(dmit)_2]^-$ arrangements having different magnitude of $t_1$-values. The diversity in the $[Ni(dmit)_2]^-$ anion arrangements were realized by introducing flexible supramolecular cation structures. In addition to previously reported (anilinium)([18]crown-6)[Ni-$(dmit)_2]_2$ (i) and (*p*-phenylenediammonium)([18]crown-6)[Ni-$(dmit)_2]_2$ (ii),[9,10] which had $\pi-\pi$ dimer structures of $[Ni(dmit)_2]^-$ anions, the relationship between the magnetic exchange energy *J*, which was estimated from magnetic susceptibility measurements, and $t_1$ values, which were estimated by extended Hückel MO calculations of salts **1a**$-$**3** was plotted. The transfer integrals were obtained by the linear relation $t = -ES$ ($E = -10$ eV), where the parameter *E* is the order of energy of LUMO. Although the absolute value of transfer integral depends on the parameter *E*, the use of constant $E = -10$ eV can reproduce a larger number of band parameters; bandwidth and Fermi surface, for the molecular conductors.[14] Thus we employed the linear relation of $t = -10S$ eV for the estimation of magnetic exchange energy *J*.

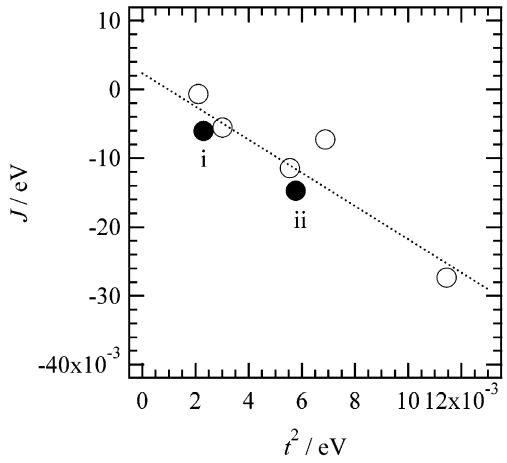


**Figure 11.** Linear correlation between the magnetic exchange energy (*J*/eV) and the square value of the intradimer transfer integral ($t^2$/eV$^2$). Data (i) and (ii) are cited from (anilinium)([18]crown-6)$[Ni(dmit)_2]$ and (*p*-phenylendiammonium)([18]crown-6)$[Ni(dmit)_2]_2$. Dashed line represents the result of the fit using equation ($J = 2t^2/U_{eff}$).

Figure 11 shows the linear correlation between the parameters *J* and $t^2$, which suggested that the intradimer $t_1$, based on the extended Hückel model, provided a rather reasonable result for a series of $[Ni(dmit)_2]^-$ anions. It has been known that band structure calculations, based on extended Hückel method, can reproduce the Fermi surface of molecular conductors.[2] From the fitting result, an important parameter of $U_{eff}$ was estimated as roughly 0.83 eV for the $[Ni(dmit)_2]^-$ anion system, whose magnitude was reasonable for the $\pi$-conjugated molecular system. The semiconducting and metallic electrical conductivities of (phenazinium)$[Ni(dmit)_2]_3$ and (acridinium)$[Ni(dmit)_2]_3$ were explained using band structure calculations according to a tight-binding model and including $U_{eff}$.[20] Both systems became metallic in character for the band structure calculation without including $U_{eff}$. The difference of the temperature-dependent electrical conductivities between the metal and semiconductor was explained by introducing an effective $U_{eff} \sim 0.8$ eV for the $[Ni(dmit)_2]$ anion system.[20] The electronic charge-transfer

excitation of the $[Ni(dmit)_2]^-$ anion was typically observed at around 1 eV in the NIR energy region, whose transition corresponded to the optical excitation from two $[Ni(dmit)_2]^-$ anions to $[Ni(dmit)_2]^0 + [Ni(dmit)_2]^{2-}$, i.e., $U_{eff}$ in the solid. The resultant $U_{eff}$ value from the eq 1 was consistent with these results.

## 4. Summary

Flexible supramolecular cation structures of $[(XyDA)_{0.5}$-(crown ethers)$]^+$ were incorporated into $[Ni(dmit)_2]^-$ salts. Hydrogen-bonding interactions between the $-CH_2-NH_3^+$ moieties of the XyDA cation and the oxygen atoms in the crown ethers yielded sandwich-type supramolecular assemblies. The two $-CH_2-NH_3^+$ arms of XyDA, which were flexible and freely rotated around the C−N bonds, offered a variety of conformations for the $[(XyDA)_{0.5}$(crown ethers)$]^+$ structures and also for the $[Ni(dmit)_2]^-$ anion arrangements in the crystals. The $[(XyDA)_{0.5}$([12]crown-4)$]^+$ complex yield three crystals, including two polymorphs of $[(XyDA)_{0.5}$([12]crown-4)$]^+[Ni(dmit)_2]$, whereas $[(XyDA)_{0.5}$([15]crown-5)$]^+[Ni(dmit)_2]$ yielded two polymorphs. Subtle rotations around the $-CH_2-NH_3^+$ arms was found to change the conformations of hydrogen-bonded $[(XyDA)_{0.5}$(crown ethers)$]^+$ supramolecular assemblies. The relatively larger [18]crown-6 molecules covered the $\pi$-plane of XyDA and prevented the formations of intermolecular interactions between the XyDA cation and $[Ni(dmit)_2]^-$ anion, and thus, only one type of $[(XyDA)_{0.5}$([18]crown-6)$]^+[Ni(dmit)_2]$ was observed. Addition of conformational flexibility to the supramolecular cation structures was considerably effective in controlling the $[Ni(dmit)_2]^-$ anion arrangement. Most of the $[Ni(dmit)_2]^-$ anions formed $\pi-\pi$ dimers, which are in the singlet ground state. The magnetic exchange energy $J$ within the dimer, i.e., intradimer interaction, was modified by the conformation of $[(XyDA)_{0.5}$(crown ethers)$]^+$ structures. The linear correlation between the value of $J$ in the dimer and the square of the intradimer transfer integral $t_1^2$, based on extended Hückel method, was obtained, which provided an estimation of the effective on-site Coulomb repulsive energy as $U_{eff} \sim 0.8$ eV for the $[Ni(dmit)_2]^-$ anion system. Structural designs using flexible cation system are currently in progress to fabricate novel $[Ni(dmit)_2]$-based molecular conductors and magnets.

**Acknowledgment.** This work was partly supported by a Grant-in-Aid for Science Research from the Ministries of Education, Culture, Sports, Science, and Technology of Japan. The authors thank Dr. M. Wakeshima, Dr. K. Ichimura, Prof. Y. Hinatsu, and Prof. K. Nomura for allowing the use of their SQUID magnetometer.

**Supporting Information Available:** Preparation of salts **1a**−**3**, temperature-dependent molar magnetic susceptibility of salt **3**, the atomic coordinates, anisotropic thermal parameters, and bond lengths for crystals **1a**−**3**. This material is available free of charge via the Internet at http://pubs.acs.org.

## References and Notes

(1) (a) Dunitz, J.; Bernstein, J. *Acc. Chem. Res*. **1995**, *28*, 193. (b) *Organized Molecular Assemblies in the Solid State*; Whitesell, J. K. Ed.; Wiley: Chichester, 1999. (c) Steed, J. W., Atwood, J. L., Eds. *Supramolecular Chemistry*; Wiley: Chichester, **2000**.

(2) (a) Williams, J. M.; Ferraro, J. R.; Thorn, R. J.; Carlson, K. D.; Geiser, U.; Wang, H. H.; Kini, A. M.; Whangbo, M.-H. *Organic Superconductors*; Grimes, R. N., Ed.; Prentice Hall: New Jersey, **1992**. (b) Ishiguro, T.; Yamaji, K.; Saito, G. *Organic Superconductors*; Fulde, P. Ed.; Springer-Verlag: New York, 1998.

(3) (a) Braga, D.; Grepioni, F.; Desiraju, G. R. *Chem. Rev*. **1998**, *98*, 1375. (b) Seiler, P.; Dunitz, J. D. *Acta Crystallogr., Sect. B* **1979**, *35*, 2020. (c) Seiler, P.; Dunitz, J. D. *Acta Crystallogr., Sect. B* **1982**, *38*, 1741. (d) Takusagawa, F.; Koetzle, T. F. *Acta Crystallogr., Sect. B* **1979**, *35*, 1074. (e) Seiler, P.; Dunitz, J. D. *Acta Crystallogr., Sect. B* **1979**, *B35*, 1068.

(4) (a) Kuroda, Y.; Taira, Z.; Uno, T.; Osaki, K. *Cryst. Struct. Commun*. **1975**, *4*, 321. (b) Matias, P. M.; Heffrey, G. A.; Ruble, J. R. *Acta Crystallogr., Sect. B*. **1988**, *44*, 516.

(5) (a) Graven, B. M.; Vizzini, E. A.; Rodrigues, M. M. *Acta Crystallogr., Sect. B*. **1969**, *25*, 1978. (b) Graven, B. M.; Vizzini, E. A. *Acta Crystallogr., Sect. B*. **1971**, *27*, 1917.

(6) Lehn, J.-M. *Supramolecular Chemistry*; Anton, U., Ed.; VCH: Weinheim, 1995.

(7) (a) Akutagawa, T.; Nakamura, T.; Inabe, T.; Underhill, A. E. *J. Mater. Chem*. **1996**, *7*, 135. (b) Akutagawa, T.; Nakamura, T.; Inabe, T.; Underhill, A. E. *Thin Solid Films* **1998**, *331*, 264. (c) Akutagawa, T.; Nakamura, T. *Coord. Chem. Rev*. **2000**, *198*, 297. (d) Akutagawa, T.; Nezu, Y.; Hasegawa, T.; Nakamura, T.; Sugiura, K.; Sakata, Y.; Inabe, T.; Underhill, A. E. *Chem. Commun*. **1998**, 2599. (e) Robertson, N.; Akutagawa, T.; Nakamura, T.; Roehrs, S.; Underhill, A. E. *J. Mater. Chem*. **1999**, *9*, 1233. (f) Akutagawa, T.; Hasegawa, T.; Nakamura, T.; Inabe, T.; Sugiura, K.; Sakata, Y.; Underhill, A. E. *Synth. Metals* **1999**, *102*, 1747. (g) Akutagawa, T.; Hasegawa, T.; Nakamura, T.; Takeda, S.; Inabe, T.; Sugiura, K.; Sakata, Y.; Underhill, A. E. *Inorg. Chem*. **2000**, *39*, 2645. (h) Nakamura, T.; Akutagawa, T.; Honda, K.; Underhill, A. E.; Coomber, A. T.; Friend, R. H. *Nature* **1998**, *394*, 159. (i) Akutagawa, T.; Hasegawa, T.; Nakamura, T.; Takeda, S.; Inabe, T.; Sugiura, K.; Sakata, Y.; Underhill, A. E. *Chem. Eur. J*. **2001**, *7*, 4902. (j) Akutagawa, T.; Hasegawa, T.; Nakamura, T.; Inabe, T. *J. Am. Chem. Soc*. **2002**, *124*, 8903.

(8) (a) Takamatsu, N.; Akutagawa, T.; Hasegawa, T.; Nakamura, T.; Inabe, T.; Fujita, W.; Awaga, K. *Inorg. Chem*. **2000**, *39*, 870. (b) Akutagawa, T.; Nishihara, S.; Takamatsu, N.; Hasegawa, T.; Nakamura, T.; Inabe, T. *J. Phys. Chem. B* **2000**, *104*, 5871. (c) Akutagawa, T.; Takamatsu, N.; Shitagami, K.; Hasegawa, T.; Nakamura, T.; Inabe, T. *J. Mater. Chem*. **2001**, *11*, 2118. (d) Takamatsu, N.; Akutagawa, T.; Hasegawa, T.; Nakamura, T.; Inabe, T.; Fujita, W.; Awaga, K. *Mol. Cryst. Liq. Cryst*. **2000**, *343*, 163. (e) Akutagawa, T.; Nakamura, T. *Coord. Chem. Rev*. **2002**, *226*, 3.

(9) Nishihara, S.; Akutagawa, T.; Hasegawa, T.; Nakamura, T. *Chem. Commun*. **2002**, 408.

(10) Nishihara, S.; Akutagawa, T.; Hasegawa, T.; Nakamura, T. *J. Solid State Chem*. **2002**, in press.

(11) (a) Weber, E.; Toner, J. L.; Goldberg, I.; Vögtle, F.; Laidler, D. A.; Stoddart, J. F.; Bartsch, R. A.; Liotta, C. L. *Crown Ethers and Analogues*; Patai, S., Rappoport, Z., Eds.; John Wiley & Sons: New York, 1989. (b) Gokel, G. W. *Crown Ethers & Cryptands*; Stoddart, J. F., Ed.; RSC: Cambridge, 1994.

(12) Steimecke, G.; Sieler, H. J.; Krimse, R.; Hoyer, E. *Phosphorus Sulfur* **1979**, *7*, 49.

(13) Crystal Structure: Single-crystal structure analysis software. Ver. 1.0, **2000**. Rigaku Corporation and Molecular Structure Corporation. For ortep drawing, Farrugia, L. J. *J. Appl. Crystallogr*. **1997**, *32*, 565.

(14) Mori, T.; Kobayashi, A.; Sasaki, Y.; Kobayashi, H.; Saito, G.; Inokuchi, H. *Bull. Chem. Soc. Jpn*. **1984**, *57*, 627.

(15) (a) Jeffrey, G. A. *An Introduction to Hydrogen Bonding*; Truhlar, D. G., Ed.; Oxford University Press: New York, 1997. (b) Pimentel, G. C.; McClellan, A. L. *The Hydrogen Bond*; Freemann: San Francisco, 1960. (c) Hamilton, W. C.; Ibers, J. A. *Hydrogen Bonding in Solid*; Breslow, R.; Karplus, M. Eds.; Benjamin Inc: New York, 1968.

(16) West, A. R. *Basic Solid State Chemistry*; Wiley: Chichester, **1988**.

(17) (*a*) Bondi, A. *J. Phys. Chem*. **1964**, *68*, 441. (*b*) Wells, A. F. *Structural Inorganic Chemistry*, 5th ed.*;* Clarendon Press: Oxford, 1984.

(18) Scott, J. C. *Semiconductor and Semimetals. High Conducting Quasi-One-Dimensional Organic Crystals*; Conwell, E., Ed.; Academic Press: New York, 1988; p 385.

(19) Carlin, R. L. *Magnetochemistry*; Springer-Verlag: Heidelberg, 1986. (b) Kahn, O. *Molecular Magnetism*; VCH: New York, 1993.

(20) (a) Paulus, P. M.; Brom, H. B.; Veldhuizen, Y. S. J.; Masskant, W. J. A. *Solid State Commun*. **1996**, *97*, 737. (b) Veldhuizen, Y. S. J.; Smeets, W. J. J.; Veldman, N.; Spek, A. L.; Faulmann, C.; Suban-Senzier, P.; Jérome, D.; Paulus, P. M.; Hassnoot, J. G.; Reedijk, J. *Inorg. Chem*. **1997**, *36*, 4930.